LETTER

doi:10.1038/nature22045

Experimental evidence that thrust earthquake ruptures might open faults

Vahe Gabuchian[1], Ares J. Rosakis[1], Harsha S. Bhat[2], Raúl Madariaga[2] & Hiroo Kanamori[3]

Many of Earth's great earthquakes occur on thrust faults[1]. These earthquakes predominantly occur within subduction zones, such as the 2011 moment magnitude 9.0 eathquake in Tohoku-Oki, Japan, or along large collision zones, such as the 1999 moment magnitude 7.7 earthquake in Chi-Chi, Taiwan[2]. Notably, these two earthquakes had a maximum slip that was very close to the surface[3,4]. This contributed to the destructive tsunami that occurred during the Tohoku-Oki event and to the large amount of structural damage caused by the Chi-Chi event. The mechanism that results in such large slip near the surface is poorly understood as shallow parts of thrust faults are considered to be frictionally stable[5]. Here we use earthquake rupture experiments to reveal the existence of a torquing mechanism of thrust fault ruptures near the free surface that causes them to unclamp and slip large distances. Complementary numerical modelling of the experiments confirms that the hanging-wall wedge undergoes pronounced rotation in one direction as the earthquake rupture approaches the free surface, and this torque is released as soon as the rupture breaks the free surface, resulting in the unclamping and violent 'flapping' of the hanging-wall wedge. Our results imply that the shallow extent of the seismogenic zone of a subducting interface is not fixed and can extend up to the trench during great earthquakes through a torquing mechanism.

As the recent 2011 moment magnitude (M_w) 9.0 Tohoku-Oki event clearly demonstrated, the shallow portion (up to several tens of kilometres down-dip from the trench axis) of a subduction zone can not only slip seismically but can also slip to a large distance of about 50 m (ref. 3). A similar observation was made during the 1999 M_w 7.7 Chi-Chi earthquake in Taiwan, during which the shallow part of the fault slipped as much as 15 m (ref. 4). The lack of shallow seismicity and laboratory evidence showing that shallow parts of these faults are frictionally stable[5] has introduced an apparent paradox about the behaviour of thrust faults in the wake of the above observations. Thrust fault events also show significant asymmetry in ground motion[6] and fracture damage across the two sides of the fault, with more damage and larger accelerations on the hanging wall compared to the footwall[7–9]. This is due to the break in symmetry of the fault geometry and interaction of the stress waves, with respect to the free surface[10–12].

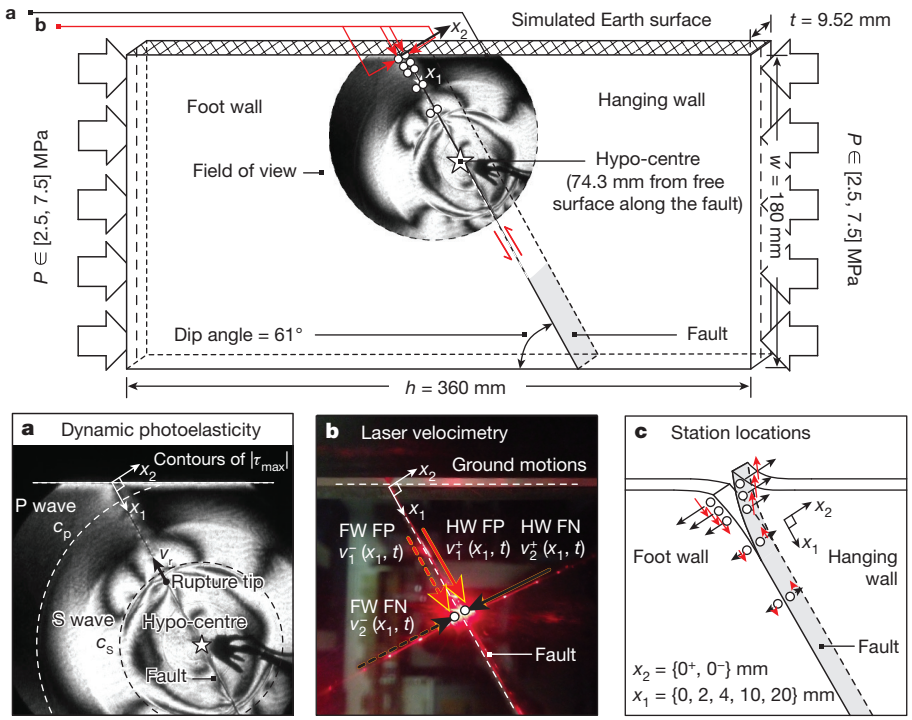

Figure 1 | A thrust fault modelled by dividing a rectangular plate with an angled cut. The schematic draws analogy to forces and geometrical elements of earthquakes. A rupture nucleates at the hypo-centre and is guided up-dip towards the simulated Earth surface. **a**–**c**, Dynamic photoelasticity (**a**) and laser velocimetry (**b**) extract full-field and discrete mechanical measurements to study free-surface effects on rupture dynamics, particularly the existence of the fault-opening phenomena (**c**). FN, fault normal; FP, fault parallel.

[1]Graduate Aerospace Laboratories, California Institute of Technology, 1200 East California Boulevard 105-50, Pasadena, California 91105, USA. [2]Laboratoire de Géologie, École Normale Supérieure, CNRS-UMR 8538, PSL Research University, Paris 75005, France. [3]Seismological Laboratory, California Institute of Technology, 1200 East California Boulevard 252-21, Pasadena, California 91105, USA.

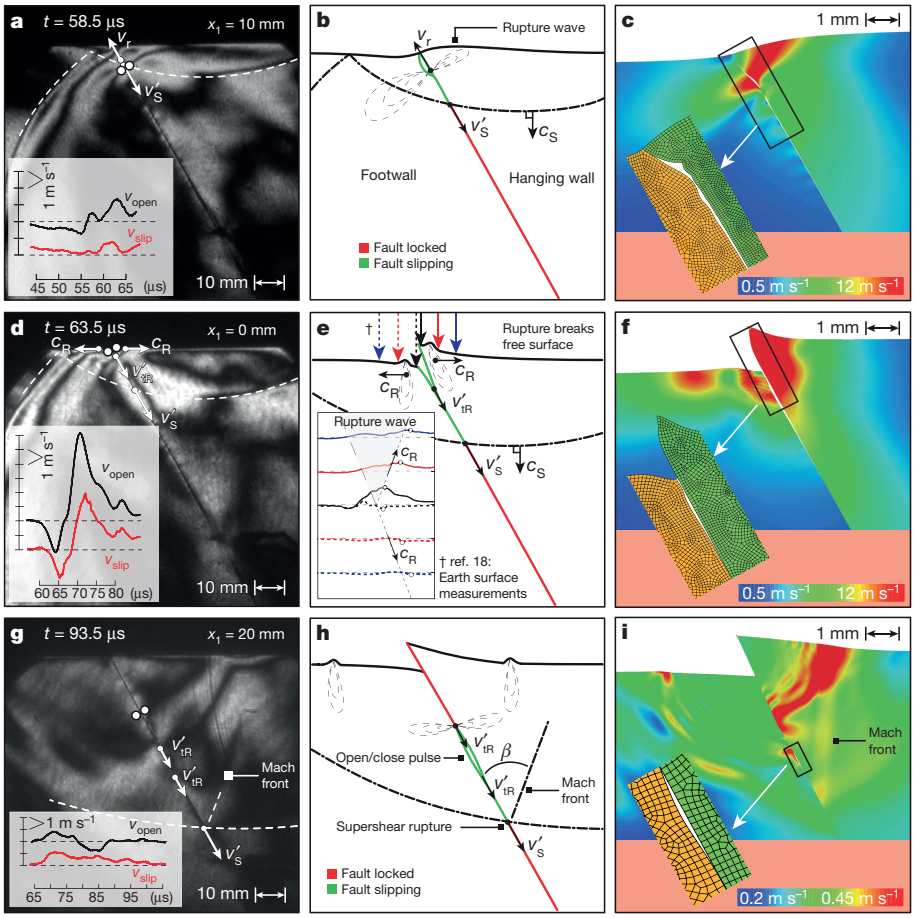

Figure 2 | A typical sub-Rayleigh rupture ($P = 2.5$ MPa) is chronologically portrayed at experimental times $t = 58.5$, 63.5, and 93.5 μs. a–i, Experimental results (**a**, **d**, **g**), schematic representations (**b**, **e**, **h**), and numerical results (**c**, **f**, **i**) summarize the simulated earthquake. The deformation in the numerical simulations is exaggerated by a factor of 40. The rupture speed (v_r) and phase velocities of bulk wave intersections with the fault are identified for both up-dip ($v_{P,S}$) and reflected down-dip phases ($v'_{P,S}$). Up-dip rupture propagation (**a**) is accompanied by opening (v_{open}) and slip pulses (v_{slip}), which are significantly amplified at the fault trace station (**d**). The reflected S wave re-ruptures the locked fault at supershear speeds ($c_S < v'_S$), emitting a Mach front (**g**). Trailing behind the down-dip rupture is an opening–shutting pulse generated at the free surface.

Brune and colleagues[13] attempted to resolve these observations and paradoxes by showing the existence of a torquing mechanism of thrust fault ruptures near the free surface in laboratory experiments conducted on foam rubber. However, foam rubber is not a suitable analogue material to represent Earth's upper crust, as it is not brittle, linear elastic, and hence this mechanism has remained unexplored. Of note, theoretical arguments from linear elastic fracture mechanics have supported this possibility[13–16]. The torquing mechanism, however, is geometrical in nature and allows for natural reduction in elastic compressive normal stress at shallow depths, up to a few kilometres down-dip a shallow subduction zone fault, owing to dynamic rupture. It even promotes fault opening in extreme situations (contrary to the assumptions of traditional theoretical and numerical models of thrust fault ruptures that the fault interface remains fully in contact during rupture). The purpose of the present work is to explore this torquing mechanism through highly instrumented, fully dynamic earthquake rupture experiments and detailed finite-element elastodynamic calculations, which allow for spontaneous fault opening.

Thrust fault rupture experiments were conducted at the Caltech Earthquake Laboratory[17] (see Methods for details). Dynamic photoelasticity and laser velocimetry were used to extract mechanical information during the simulated earthquake rupture (Fig. 1).

Three snapshots of a laboratory thrust earthquake (tectonic pressure (P) = 2.5 MPa, fault dip = 61°) collectively elucidate the rupture dynamics: experimental results (Fig. 2a, d, g), accompanying schematics (Fig. 2b, e, h), and the output of the numerical calculations mimicking experimental conditions (Fig. 2c, f, i). At around 58.5 μs after nucleation, the rupture tip arrives to station $x_1 = 10$ mm (Fig. 2a, white circles), as indicated by a rise in the recorded slip and opening velocities. Minute negative opening rates measured ahead of the rupture tip imply pinching of the interface before the concurrent initiation of both opening and slip. The fault re-locks after the rupture tip sweeps past the stations; however, reflected P and S waves from the free surface feed back stress waves onto the fault and introduce additional features in the records. In the schematic (Fig. 2b), red and green portions of the fault signify locked and slipping regions, respectively. These locked and slipping regions can be clearly seen in the numerical simulation (Fig. 2c). The up-dip propagating left-lateral rupture induces a counterclockwise torque on the hanging-wall wedge.

At around 63.5 μs, the rupture tip arrives at the free surface, $x_1 = 0$ mm, breaking the simulated Earth surface (Fig. 2d). The recorded slip and opening velocities (v) exhibit significant amplification in peak values at the free surface ($v_{slip}^{max} \approx 4$ m s^{-1} and $v_{open}^{max} \approx 6$ m s^{-1}). Peak negative values associated with the pinching precursor are also amplified and are at this stage accompanied by an in-phase negative slip signature, both approximately equal to -2 m s^{-1}. Numerical simulations suggest that the above effect is due to the release of the counterclockwise torque that has built up on the hanging-wall wedge before the rupture breaks the free surface (Fig. 2f). Owing to the absence of material above the free surface, the fault is unable to counteract the pinching motion ahead of the rupture, resulting in immediate compression and release of the stress on the interface through opening and

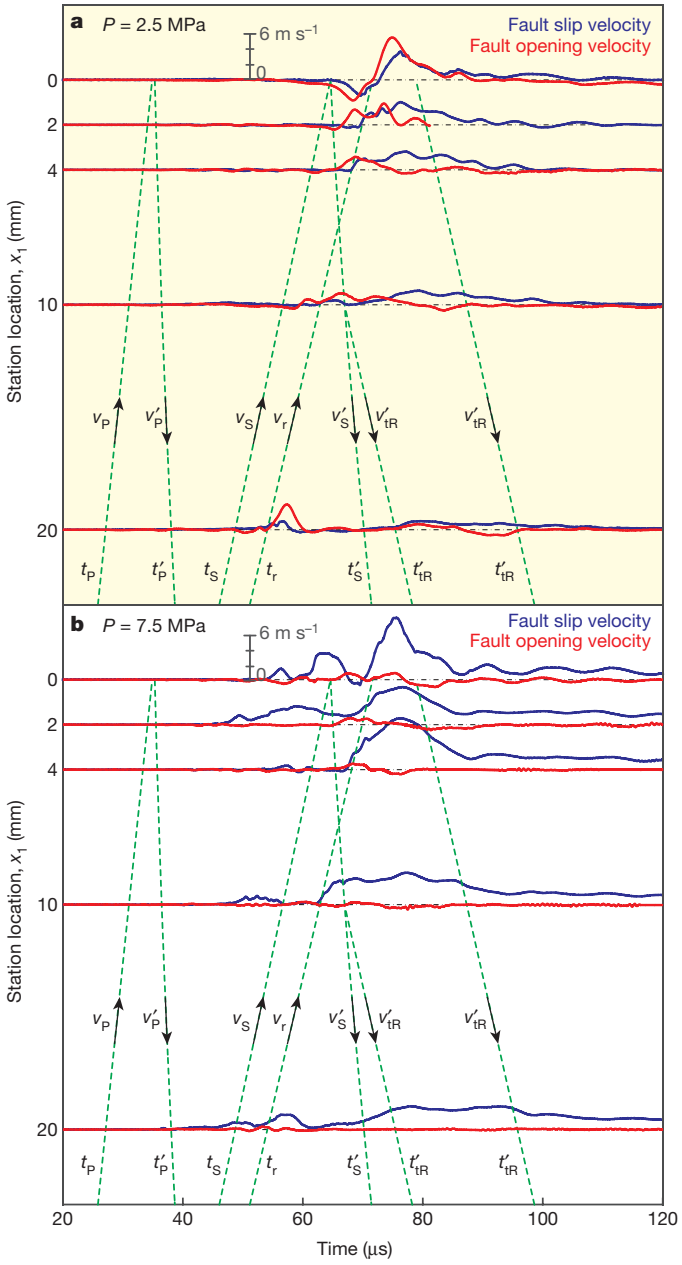

Figure 3 | Recorded fault slip (v_{slip}) and opening velocity (v_{open}). **a**, **b**, Measured at stations $x_1 = 0$, 2, 4, 10, 20 mm along the fault for both experimental loads $P = 2.5$ MPa (**a**) and 7.5 MPa (**b**). Up-dip rupture tip arrival, t_r, induces a slip pulse for both loads; however, the opening pulse is attenuated in the higher-load experiment. The down-dip supershear rupture, t'_r, is pulse-like for $P = 2.5$ MPa and crack-like for $P = 7.5$ MPa experiments: increased confinement loads enhance slip but inhibit fault opening. Ground motions amplify towards the free surface as the up-dip and down-dip ruptures coalesce, elongating the slip and opening velocity pulses for stations within $x_1 \approx 10$ mm.

slip. Separation of the fault surfaces generates an opening pulse propagating down-dip at speed v'_{tR} and two surface Rayleigh waves travelling, with a velocity c_R, on either side of the fault, along the simulated Earth surface (Fig. 2e, daggered insert); the latter claim has been verified with previous measurements along the free surface[18]. The opening pulse trails behind the reflected S-wave front and propagates at $v'_{tR} = 1.20\,\mathrm{km\,s^{-1}} \approx c_R$. Oscillations in the records persist past the arrival of the rupture tip, extending the slip and opening process durations near the free surface. Theoretical work on thrust faults discusses the instantaneous emergence of a Boussinesq point force at the fault trace: the sudden inability of the system to sustain a moment upon rupture tip arrival to the free surface is balanced by this point force[12]. The measured fault-opening phenomenon is strong evidence in support of this claim.

At the deepest station, $x_1 = 20$ mm, at time $t = 68.5\,\mu$s, recorded slip and velocity indicate that the reflected S-wave front re-ruptures the fault (Fig. 2g). The photograph at $t = 93.5\,\mu$s shows a shear Mach front emanating from the intersection of the reflected S wave and the fault, that is, the rupture tip ($v'_S = v'_r$). Measurements from consecutive frames confirm that the average rupture tip speed is indeed supershear, $v'_r \approx 1.6\,\mathrm{km\,s^{-1}}$ (1.24 c_S). The geometric relation $v'_r(\beta) = c_S / \sin\beta$ and Mach angle $\beta = 47°$ verify supershear speeds $v'_r(47°) \approx 1.7\,\mathrm{km\,s^{-1}}$. Trailing behind the down-dip rupture are the pair of fringes that correspond to the opening and shutting of the fault at the free surface (v'_{tR}), as seen in the opening velocity records. In fact, the numerical simulations reveal that the trailing-Rayleigh pulse is mixed mode in nature, having both both opening and slipping modes (Fig. 2i). The down-dip supershear slip pulse has larger slip velocity than the up-dip rupture slip pulse (Fig. 2h), due to the fact that a downward propagating rupture (which can be roughly seen as an upward propagating rupture reflecting off of the free surface) now encounters a region of much lower frictional resistance. This leads to greater slip rates in the down-dip direction. Because of this reduced frictional resistance, we expect the down-dip supershear rupture to exist at higher confining stresses.

Fault slip and opening velocity records measured at stations $x_1 = 0$, 2, 4, 10, 20 mm are collectively plotted in Fig. 3 for experimental loads $P = 2.5$ MPa and $P = 7.5$ MPa. Timing lines bound the arrivals of up-dip P (and S) waves, $t_{P,S}$, up-dip rupture tip, t_r, down-dip P (S) waves, $t'_{P,S}$, and the down-dip trailing Rayleigh signatures, t'_{tR}. In the $P = 2.5$ MPa data set (Fig. 3a), before the arrival of the first reflected P wave ($t < t'_P$), the rupture process is blind to the presence of the free-surface boundary. Reflected P waves continuously feed back onto the fault with nearly no effect on the slip and opening velocity. However, the reflected S-wave front, with an arrival time of t'_S, re-ruptures the fault as it propagates back down-dip. This is clearly seen for station $x_1 = 20$ mm at around $t = 70\,\mu$s. Although the up-dip rupture is sub-Rayleigh, $0 < v_r < c_R$, appearance of shear Mach fronts (Fig. 2g) and the geometry-driven inequality, $c_S < v'_S$, together validate the existence of a down-dip supershear rupture, $c_S < v'_r < c_P$. For stations within $x_1 \approx 10$ mm, the up-dip and down-dip ruptures coalesce, broadening the slip–velocity pulse near the free surface. In response to the opening and subsequent shutting of the fault at the free surface, the system sends an opening–closing pulse back down-dip at the Rayleigh wave speed (timing lines t'_{tR} correspond to the leading and trailing edges). The leading supershear slip pulse t'_S is broadened by the decrease in normal stress of the fault from this trailing-Rayleigh signature. Oscillations in the records after rupture tip arrival are unique to stations near the free surface. The recorded slip and opening velocity for $P = 7.5$ MPa experiments (Fig. 3b) show similar results, with several key differences. The magnified driving shear stress enhances slip at every station. The fault has a lower tendency to lock; in fact, the down-dip supershear rupture is crack-like rather than pulse-like. Whereas slip is enhanced, fault opening is nearly absent in the higher-load experiments, except very close to the free surface. Unlike in the $P = 2.5$ MPa results, the down-dip opening–closing pulse is absent in the $P = 7.5$ MPa records, showing that higher confinement loads tend to enhance slip and suppress opening. It is worth noting that amplification of slip and opening rates near the free surface is largely due to the preferential enhancement of hanging-wall ground motions for both parallel and normal components of the fault.

High-resolution, controlled experimental and numerical results conclusively validate the hypothesis that certain thrust faults (collisional and subduction) suffer significant reduction in compressional normal stress owing to free surface effects and that they might open when an up-dip propagating rupture breaks that surface. This reduction in normal stress is essentially a geometrical phenomenon that is

expressed whenever a dynamic rupture runs through a thrust fault and approaches the surface of the earth. The 2011 Tohoku-Oki earthquake occurred on a bimaterial interface where the material on the hanging wall was softer than that on the footwall[19,20]. This naturally results in reduction of normal stress around the up-dip propagating rupture. The mechanism that we propose, when correctly accounted for in the numerical models, will further reduce the normal stress, making the possibility of opening even more likely. Indeed, any other physical mechanism that is invoked to reduce normal stress, when coupled with the mechanism we propose, would only enhance the effect of normal stress reduction as our mechanism is geometrical in nature.

The laboratory experiments show that there is a small, but non-negligible, opening at confining pressure of $P = 7.5$ MPa. This corresponds to a normal stress of $\sigma = 5.7$ MPa that acts on the fault plane. It can be shown, using reasonable values of the state of stress in fluid-rich sedimentary upper crust[21], that the corresponding down-dip extent l along a shallow subduction fault ($5^o < \text{dip}\ (\delta) < 10^o$), where the normal stress corresponds to laboratory conditions, is between 2 km and 4 km ($l \approx 6.10^{-5}\sigma / \sin\delta$). These correspond to depths at which large shallow slip was observed in the 1999 Chi-Chi earthquake, around 15 m, and the 2011 Tohoku-Oki earthquake, around 50 m. Further evidence of fault opening comes from the lack of high-frequency radiation from the shallow part of the thrust ruptures, observed for both the Tohoku-Oki[22] and the Chi-Chi[7,23] earthquakes. Geological evidence for this mechanism has been observed during the Chi-Chi earthquake, when the toe of the fault was propelled forward and crumpled during its passage, with no overshoot[7]. During the 1971 San Fernando Earthquake, a large volume of asphalt covering the surface trace of the thrust fault was seemingly coherently translated about 1.5 m by motions associated with thrust-fault displacement[24]. High-resolution mapping of the 2013 M_w 7.7 Balouchistan earthquake (dominant strike-slip with local dip-slip component) shows significant tensile cracks on certain sections of the hanging wall of the fault[9]. This fault had an average dip angle of approximately 60°, as in our experiments. These latter observations may be explained by the mechanism we propose, by which the hanging wall undergoes significant rotations in both directions as the rupture approaches and breaks the free surface, resulting in complete reduction of compressive normal stress.

Once the rupture breaks the free surface, it reverses course and propagates down-dip as a supershear rupture (with higher slip rates) that is trailed by an opening and a sliding pulse, which propagates at the Rayleigh wave speed. This effect could explain the observed enhanced slip pulse propagating down-dip during the Tohoku-Oki earthquake[22,25].

In conclusion, this work shows that accounting for this mechanism of dynamic normal stress reduction, with possible opening, along with dynamic frictional weakening processes and bimaterial effects, helps to resolve the majority of the paradoxes associated with surface-breaking earthquakes in thrust faults.

Online Content Methods, along with any additional Extended Data display items and Source Data, are available in the online version of the paper; references unique to these sections appear only in the online paper.

Received 5 September 2016; accepted 1 March 2017.
Published online 1 May 2017.

1. Dixon, T. H. & Moore, J. C. *The Seismogenic Zone of Subduction Thrust Faults* (Columbia Univ. Press, 2007).
2. Tanaka, H. *et al.* Frictional heat from faulting of the 1999 Chi-Chi, Taiwan earthquake. *Geophys. Res. Lett.* **33,** L16316 (2006).
3. Fujiwara, T. *et al.* The 2011 Tohoku-Oki earthquake: displacement reaching the trench axis. *Science* **334,** 1240–1240 (2011).
4. Ma, K.-F., Mori, J., Lee, S.-J. & Yu, S. Spatial and temporal distribution of slip for the 1999 Chi-Chi, Taiwan, earthquake. *Bull. Seismol. Soc. Am.* **91,** 1069–1087 (2001).
5. Saffer, D. M. & Marone, C. Comparison of smectite-and illite-rich gouge frictional properties: application to the updip limit of the seismogenic zone along subduction megathrusts. *Earth Planet. Sci. Lett.* **215,** 219–235 (2003).
6. Abrahamson, N. A. & Somerville, P. G. Effects of the hanging wall and footwall on ground motions recorded during the Northridge earthquake. *Bull. Seismol. Soc. Am.* **86,** S93–S99 (1996).
7. Bilham, R. & Yu, T.-T. The morphology of thrust faulting in the 21 September 1999, Chichi, Taiwan earthquake. *J. Asian Earth Sci.* **18,** 351–367 (2000).
8. Brune, J. N. Shattered rock and precarious rock evidence for strong asymmetry in ground motions during thrust faulting. *Bull. Seismol. Soc. Am.* **91,** 441–447 (2001).
9. Vallage, A., Klinger, Y., Grandin, R., Bhat, H. S. & Pierrot-Deseilligny, M. Inelastic surface deformation during the 2013 M_w 7.7 Balochistan, Pakistan, earthquake. *Geology* **43,** 1079–1082 (2015).
10. Savage, J. C. The stopping phase on seismograms. *Bull. Seismol. Soc. Am.* **55,** 47–58 (1965).
11. Oglesby, D. D., Archuleta, R. J. & Nielsen, S. B. Earthquakes on dipping faults: the effects of broken symmetry. *Science* **280,** 1055–1059 (1998).
12. Madariaga, R. Radiation from a finite reverse fault in a half space. *Pure Appl. Geophys.* **160,** 555–577 (2003).
13. Brune, J. N. Particle motions in a physical model of shallow angle thrust faulting. *Proc. Indian Acad. Sci. (Earth Planet. Sci.)* **105,** L197–L206 (1996).
14. Erdogan, F. & Arin, K. A half plane and a strip with an arbitrarily located crack. *Int. J. Fract.* **11,** 191–204 (1975).
15. Dmowska, R. & Rice, J. R. in *Continuum Theories in Solid Earth Physics. Physics and Evolution of the Earth's Interior* Vol. 3 (ed. Teisseyre, R.) (Elsevier, 1986).
16. Rudnicki, J. W. & Wu, M. Mechanics of dip-slip faulting in an elastic half-space. *J. Geophys. Res.* **100,** 22173–22186 (1995).
17. Xia, K., Rosakis, A. J. & Kanamori, H. Laboratory earthquakes: the sub-Rayleigh-to-supershear rupture transition. *Science* **303,** 1859–1861 (2004).
18. Gabuchian, V., Rosakis, A. J., Lapusta, N. & Oglesby, D. D. Experimental investigation of strong ground motion due to thrust fault earthquakes. *J. Geophys. Res.* **119,** 1316–1336 (2014).
19. Kozdon, J. E. & Dunham, E. M. Rupture to the trench: dynamic rupture simulations of the 11 March 2011 Tohoku earthquake. *Bull. Seismol. Soc. Am.* **103,** 1275–1289 (2013).
20. Scholz, C. H. The rupture mode of the shallow large-slip surge of the Tohoku-Oki earthquake. *Bull. Seismol. Soc. Am.* **104,** 2627–2631 (2014).
21. Suppe, J. Fluid overpressures and strength of the sedimentary upper crust. *J. Struct. Geol.* **69,** 481–492 (2014).
22. Ide, S., Baltay, A. & Beroza, G. C. Shallow dynamic overshoot and energetic deep rupture in the 2011 M_w 9.0 Tohoku-Oki earthquake. *Science* **332,** 1426–1429 (2011).
23. Ma, K.-F. *et al.* Evidence for fault lubrication during the 1999 Chi-Chi, Taiwan, earthquake (M_w 7.6). *Geophys. Res. Lett.* **30,** 1244 (2003).
24. Allen, C. R., Brune, J. N., Cluff, L. S. & Barrows, A. G. Evidence for unusually strong near-field ground motion on the hanging wall of the San Fernando fault during the 1971 earthquake. *Seismol. Res. Lett.* **69,** 524–531 (1998).
25. Huang, Y., Meng, L. & Ampuero, J.-P. A dynamic model of the frequency-dependent rupture process of the 2011 Tohoku-Oki earthquake. *Earth Planets Space* **64,** 1061–1066 (2012).

Acknowledgements We gratefully acknowledge the National Science Foundation (award number EAR-1321655), which has supported this research. We also acknowledge our colleague, N. Lapusta (California Institute of Technology) for comments and advice. H.S.B. acknowledges K. Kiara and A. Schubnel for inspiring this work.

Author Contributions A.J.R., R.M. and H.S.B. concieved the study and designed the experiments. V.G. and A.J.R. conducted the experiments. R.M. and H.S.B. conducted numerical modelling studies. All authors contributed to analysis, interpretation and manuscript preparation.

Author Information Reprints and permissions information is available at www.nature.com/reprints. The authors declare no competing financial interests. Readers are welcome to comment on the online version of the paper. Publisher's note: Springer Nature remains neutral with regard to jurisdictional claims in published maps and institutional affiliations. Correspondence and requests for materials should be addressed to H.S.B. (bhat@geologie.ens.fr).

Reviewer Information *Nature* thanks C. Scholz and the other anonymous reviewer(s) for their contribution to the peer review of this work.

METHODS

Thrust fault rupture experiments were conducted at the Caltech Earthquake Laboratory facility[17]. This facility and setup is the same used by Gabuchian *et al.* in the previous publications[18]. In this setup, dynamic photoelasticity (Fig. 1a) and laser velocimetry (Fig. 1b) are used to record deformations occurring during the simulated earthquake ruptures. Digital cameras capture a sequence of images with 50 ns exposure times, providing a full-field view of the rupture process. Photoelasticity yields isochromatic fringe patterns related to magnitudes of maximum shear stress averaged through the thickness of the specimen, $|\tau_{max}(x_1, x_2, t)|$. Complementary use of full-field images and discrete velocity records identifies the effects of various dynamic features of ground motion and slip history. The laser velocimeter systems function as laboratory seismometers, each outputting a temporally resolved velocity record for a single component of ground motion at a discrete point on the specimen[26].

A thrust fault is modelled in the laboratory by means of a rectangular plate with dimensions height = 360 mm, width = 180 mm, and thickness = 9.52 mm (Fig. 1). The surrogate material is Homalite H-100, a brittle linear elastic, transparent, optically bi-refringent polymer with the dilatational (P) wave speed, $c_P = 2.59\,km\,s^{-1}$ and the shear (S) wave speed $c_S = 1.27\,km\,s^{-1}$. An angled cut divides the specimen into the hanging wall and footwall plates: this interface represents a thrust fault with a 61° dip angle. We can currently model only steep faults in the laboratory, but in the future maybe be able to model shallower faults; this would have a direct application to the physics of shallow thrust faults in the earth.

The characteristic double-lobe fringe structure trailing behind the S wave (Fig. 1a) is the signature of a sub-Rayleigh rupture tip propagating up-dip with a nearly constant speed, $v_r = 1.14\,km\,s^{-1}$ ($< c_R = 1.18\,km\,s^{-1}$, the Rayleigh wave speed). The origin of the coordinate system is set at the intersection of the fault with the free surface with the x_1 component collinear to the fault ($x_2 = 0$). The two surfaces are frictionally held together and the resulting interface experiences compression and shear under the action of the remote load. Far-field uniaxial compression of the plate mimics far-field tectonic stress in the earth: the applied load, P (MPa), resolves into fault parallel (x_1) and normal (x_2) components along the angled interface. At a distance $x_1 = 74.3$ mm from the free surface, a pre-fabricated notch houses a NiCr wire of diameter 127 μm. Discharge of a capacitor bank across the wire converts the filament to plasma, locally decreasing the fault strength such that the driving shear stress is sufficient to initiate slip. This mechanism nucleates a bilateral rupture propagating away from the hypo-centre (Fig. 1, marked by a star). Confined to the fault plane, the rupture tips unzip the fault, continuously emitting P and S stress waves into the bulk, and this process simulates an earthquake[17].

By focusing four different velocimeters just to the left and right of the fault at an offset distance, $\varepsilon \approx 200 - 300\,\mu m$, four components of ground motion are recorded in each experiment: two fault parallel, $v_1(x_1, x_2 = 0 \pm \varepsilon, t) = v_1^{\pm}(x_1)$, and two fault normal, $v_2(x_1, x_2 = 0 \pm \varepsilon, t) = v_2^{\pm}(x_1)$ components of particle velocity. For any given along-fault distance x_1, slip and opening rates are determined by taking the difference between the paired hanging wall and footwall station records: $v_{slip} = v_1^+ - v_1^-$ and $v_{open} = v_2^+ - v_2^-$. Rupture evolution is tracked by a series of experiments with measurements conducted at distances $x_1 = 0$, 2, 4, 10, 20 mm along the fault (Fig. 1c) for applied loads of $P = 2.5$ MPa and $P = 7.5$ MPa.

The numerical simulations were conducted using a commercial finite element software, ABAQUS (Dassault Systèmes Simulia Corp.), using a kinematic contact algorithm. The frictional constitutive response is modelled using a slip-weakening law with static friction, $f_s = 0.6$, dynamic friction, $f_d = 0.2$, and critical slip, $D_c = 10\,\mu m$ (ref. 27). Elastic properties, loading and frictional parameters were chosen to closely represent the laboratory earthquake. In addition to sliding, the simulation allows for the possibility of opening across the fault. The aim of the simulation is to qualitatively explain the experiments at this stage.

Data availability. All relevant data are available from the authors upon reasonable request.

26. Lykotrafitis, G. & Rosakis, A. J. Sliding along frictionally held incoherent interfaces in homogeneous systems subjected to dynamic shear loading: a photoelastic study. *Int. J. Fract.* **140,** 213–233 (2006).
27. Lu, X., Lapusta, N. & Rosakis, A. J. Analysis of supershear transition regimes in rupture experiments: the effect of nucleation conditions and friction parameters. *Geophys. J. Int.* **177,** 717–732 (2009).